HYPOTHESIS TEST FOR THE DETECTION OF MOVING TARGETS IN AUTOMOTIVE RADAR

Conference Paper · November 2017

CITATION
1

READS
17

6 authors, including:

Christopher Grimm
HELLA Group
5 PUBLICATIONS **1** CITATION
SEE PROFILE

Tai Fei
HELLA Group
14 PUBLICATIONS **22** CITATIONS
SEE PROFILE

Ernst Warsitz
HELLA Group
16 PUBLICATIONS **170** CITATIONS
SEE PROFILE

Reinhold Haeb-Umbach
Universität Paderborn
191 PUBLICATIONS **2,620** CITATIONS
SEE PROFILE

HYPOTHESIS TEST FOR THE DETECTION OF MOVING TARGETS IN AUTOMOTIVE RADAR

Christopher Grimm, Tobias Breddermann, Ridha Farhoud, Tai Fei, Ernst Warsitz
Hella KGaA Hueck & Co, 59555 Lippstadt, Germany
Email: {christopher.grimm, tobias.breddermann, ridha.farhoud, tai.fei, ernst.warsitz}@hella.com

Reinhold Haeb-Umbach
Department of Communication Engineering
University of Paderborn
33098 Paderborn, Germany
Email: haeb@nt.uni-paderborn.de

***Abstract*—In this paper, we present a hypothesis test for the classification of moving targets in the sight of an automotive radar sensor. For this purpose, a statistical model of the relative velocity between a stationary target and the radar sensor has been developed. With respect to the statistical properties a confidence interval is calculated and targets with relative velocity lying outside this interval are classified as moving targets. Compared to existing algorithms our approach is able to give robust classification independent of the number of observed moving targets and is characterized by an instantaneous classification, a simple parameterization of the model and an automatic calculation of the discriminating threshold.**

I. INTRODUCTION

The detection of moving targets in the radar field, also known as moving target indication (MTI), has been a major research field at least since the development of ground mapping radar imaging techniques for military purposes. Here, moving targets lead to a degradation of image quality, see [1], since the image synthesis is based on the assumption of stationary targets and moving targets must be elliminated. By investigating the energy distribution in images generated by Synthetic Aperture Radar (SAR) one can generate hypothesis to identify dynamic targets, see e.g. [2], [3] [4].

For automotive radars, the classification of traffic objects is an essential task, since dedicated control functions are necessary especially in the context of highly automated driver assistance functions [5]. Therefore these functions need extensive information about the surrounding objects like their size, position, class and trajectory.

Since radar signal processing offers just a limited measurement space with geometric (relative distance and angle of arrival) and kinematic (relative velocity) states, an appropriate model for accurate classification is necessary and SAR based MTI algorithms can not be applied. One example where kinematic information is being used is the human gait detection, where doppler-shifts („Micro-Doppler“), introduced by the different oscillating body parts of a human when walking through a radar beam, are detetcted, see [6] [7]. However, a certain amount of oscillation is mandatory in order to discriminate pedestrians from rigid moving targets. In this paper, we present a simple method for the discrimination of stationary and moving targets in the vehicle environment without further classification of moving targets. The proposed algorithm can thus be understood as the primary stage of more complex classification approaches. It is characterized by a simple parametrization capability and enables instantaneous classifications due to an exclusively forward-directed inference, while existing approaches classify stationary targets with more complex tracking approaches [8] [9] or otherwise use a iterative and thus computational expensive RANSAC approach [10] which searches for major group of targets and classifies them as stationary, thus is easily fooled if the majority of targets stem from moving objects.

II. STATIONARY TARGET HYPOTHESIS

A. Model Synthesis

Modern automotive radar sensors are capable of resolving the relative distance ${}^{R}\vec{r}_P(t)$, the relative velocity ${}^{R}\dot{\vec{r}}_P(t)$ and the angle of arrival ${}^{R}\phi_S$ of a targets P in sight. S describes the sensor coordinate system with ${}^{S}x$ being sensor normal and R the coordinate system which is pointing towards the target P, as drawn in fig. 1.

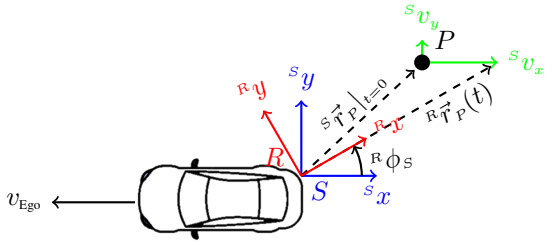

Figure 1: Coordinate transformation from sensor coordinates (S) to relative and tangential components coordinate system (R)

With the knowledge of the proper motion of the radar platform, these quantities allow mathematical formulation of targets to be derived. Here, a purely translational movement between two objects in the plane is given. The initial position is expressed by ${}^{S}\vec{r}_P|_{t=0}$, the velocity vector by the components

${}^{S}v_x$ and ${}^{S}v_y$, the angle of arrival ${}^{R}\phi_S$ in azimuth of the target P, and the time t.

$$ {}^{R}\vec{r}_P(t) = \begin{pmatrix} \cos({}^{R}\phi_S) & \sin({}^{R}\phi_S) \\ -\sin({}^{R}\phi_S) & \cos({}^{R}\phi_S) \end{pmatrix} \left({}^{S}\vec{r}_P|_{t=0} + \begin{pmatrix} {}^{S}v_x \\ {}^{S}v_y \end{pmatrix} t \right) \tag{1} $$

Since we assume a pure translational movement between the objects, the velocity vector in R can be given as

$$ \begin{pmatrix} {}^{R}v_x \\ {}^{R}v_y \end{pmatrix} = \frac{\partial {}^{R}\vec{r}_P}{\partial t} = \begin{pmatrix} {}^{S}v_x \cdot \cos({}^{R}\phi_S) + {}^{S}v_y \cdot \sin({}^{R}\phi_S) \\ -{}^{S}v_x \cdot \sin({}^{R}\phi_S) + {}^{S}v_y \cdot \cos({}^{R}\phi_S) \end{pmatrix}. \tag{2} $$

In eq. 2, the upper line describes the radial and the lower line the tangential component of the velocity.

Assuming that the incoming reflection is a stationary target and the antenna platform moves exclusively in the ${}^{S}x$ direction with a velocity ${}^{S}v_x = v_{\text{Ego}}$, that is a rectilinear motion, the measured radial velocity between the radar sensor and the reflector ${}^{R}v_x$ can be given as

$$ {}^{R}v_x = v_{\text{Ego}} \cdot \cos({}^{R}\phi_S). \tag{3} $$

The quantities ${}^{R}v_x$ and ${}^{R}\phi_S$ are measured by the radar sensor and the ego velocity v_{Ego} by the wheel speed encoders of the ego vehicle transmitted via vehicles signal interface. If eq. 3 is violated, the target may unlikely be a stationary target.

Since these quantities are generally noisy, eq. 3 usually also fails with stationary targets. There is the necessity to model the variables as statistical random variables and to specify tolerance intervals by which the measured velocity for a stationary target may deviate to some specified degree of probability.

The velocity of the ego car under investigation is given by v_{Ego}, which is usually been estimated by the product of the parametrized tire diameter and the wheels angular velocity, measured by the wheel speed encoders. The velocity estimate is degraded by stochastic error due to sensor measurement fluctuations, which we assume to be Gaussian distributed, centered at the actual velocity value $\mu_{v_{Ego}}$ of the vehicle and scaled with the variance $\sigma^2_{v_{\text{Ego}}}$. We choose Gaussian distribution as a model for V_{Ego} since the central limit theorem tells us, that a sum of independet arbitrarily distributed random variables converges always towards a Gaussian distribution [11].

$$ p_{V_{\text{Ego}}}(v_{\text{Ego}}|\mu_{V_{\text{Ego}}}, \sigma^2_{V_{\text{Ego}}}) = \frac{1}{\sqrt{2\pi\sigma^2_{V_{\text{Ego}}}}} e^{-\frac{(v_{\text{Ego}} - \mu_{V_{\text{Ego}}})^2}{2\sigma^2_{V_{\text{Ego}}}}} \tag{4} $$

For the identification of $p_{V_{\text{Ego}}}(v_{\text{Ego}}|\mu_{V_{\text{Ego}}}, \sigma^2_{V_{\text{Ego}}})$ and its parameters we drove with stationary ego-velocity of approximately $10\,\mathrm{m\,s^{-1}}$ on a straight path, measured the velocity output from vehicle signal interface and compared it to the velocity measured by a precise Differential Global Positioning System with Inertial Navigation System (DGPS-INS). The residuals of the velocity were calculated and $p_{V_{\text{Ego}}}$ was calculated as the resulting histogram. The parameters of the corresponding Gaussian distributed probability density function were also calculated by means of maximum likelihood estimation (MLE). The

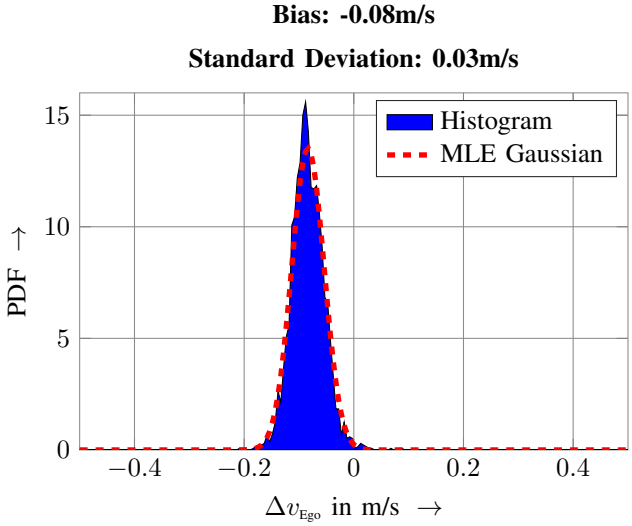

Figure 2: Centralized Probability Density Function of observing ego-velocity v_{Ego} from measurements (histogram) and from Maximum Likelihood Estimation (red)

histogram and the MLE identification are shown in fig. 2. The good match between histogram and identification confirms the modeling of $p_{V_{\text{Ego}}}$ as a Gaussian distributed random variable. The default deviation was identified as $\sigma_{V_{\text{Ego}}} = 0.03\,\mathrm{m\,s^{-1}}$. In addition, a bias of $-0.08\,\mathrm{m\,s^{-1}}$ was identified, which needs to be subtracted from the measured velocity $\mu_{V_{\text{Ego}}}$ from every realization. It is important to mention, that the identified PDF corresponds just to the here observed ego-car and could look different for another car or at future time due mechanical components wearout of the ego-car e.g. tires. It is also likely, that the bias is variant to v_{Ego}. However, for sake of simplicity we assume the bias to be constant.

As a further Gaussian distributed random variable, the radar measured variable Φ which indicates the measured angle of arrival of the raw target reflection in the ego coordinate frame, is being modeled. The actual angle of arrival is used as the mean value μ_Φ, by which the measured value is scaled with the variance σ^2_Φ

$$ p_\Phi(\phi|\mu_\Phi, \sigma^2_\Phi) = \frac{1}{\sqrt{2\pi\sigma^2_\Phi}} e^{-\frac{(\phi - \mu_\Phi)^2}{2\sigma^2_\Phi}}. \tag{5} $$

To identify $p_\Phi(\phi|\mu_\Phi, \sigma^2_\Phi)$ for the radar sensor under investigation a point-shaped target („corner reflector“) with a distance of $20\,\mathrm{m}$ was illuminated while the vehicle was in parking position ($v_{\text{Ego}} = 0\,\mathrm{m\,s^{-1}}$) over a period of $3\,\mathrm{min}$ in an otherwise empty scenario for different azimuth angles. After the recording, significant reflectors in sight were being detected and their angle of arrival have been computed. The histogram and the MLE identification for every azimuth setup were identified and just the one with the highest angle uncertainty ($\sigma_\Phi = 0.96°$) was picked for later paramatrization (histogram and identification shown in fig. 3), since this marks the worst case scenario. Some gaps in the histogram are observable, which are caused by rounding errors due to data type conversions

in angle calculation. It should be noted that the modeling as a Gaussian distributed random variable also leads to a representative distribution density.

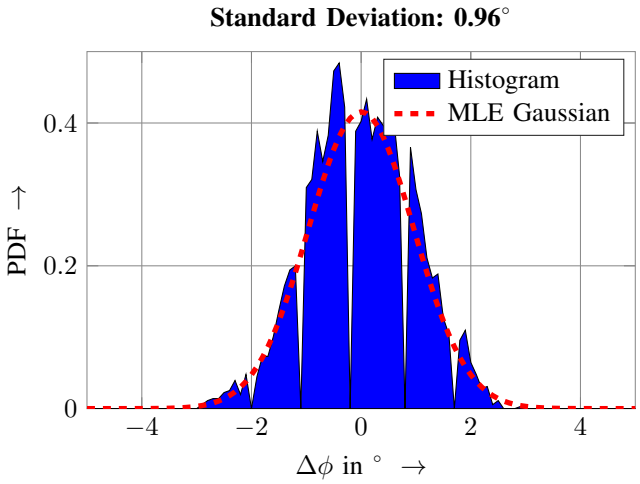

Figure 3: Probability Density Function of observing angle of arrival ϕ from measurements (histogram) and from Maximum Likelihood Estimation (red)

Lastly the remaining variable ${}^{R}v_x$ is also modeled as Gaussian, since this will provide convenient calculus as can be seen later

$$p_{R_{v_x}}({}^{R}v_x|\mu_{R_{V_x}},\sigma^2_{R_{V_x}}) = \frac{1}{\sqrt{2\pi\sigma^2_{R_{V_x}}}} e^{-\frac{({}^{R}v_x-\mu_{R_{V_x}})^2}{2\sigma^2_{R_{V_x}}}}. \quad (6)$$

We identified the parameters of this probability density function by recording stationary targets whilst standing still with the radar sensors over a period of 3 min. The histogram and the MLE identification of the recorded relative velocities are shown in fig. 4. This resulted in the standard deviation of roughly $\sigma_{R_{V_x}} = 0.01\,\mathrm{m\,s^{-1}}$. It should be mentioned, that the digital resolution lies within the estimated standard deviation, thus approximating as a continuous function introduces some source of error, which is not paid attention to further on due to the comparable small uncertainty in ${}^{R}v_x$.

Assuming that the random variables V_{Ego} and Φ are independent and the angle interval is limited to $-\frac{\pi}{2} \leq \phi \leq \frac{\pi}{2}$, their compound distribution results in

$$\begin{aligned} p_{V_{\text{Ego}},\cos(\Phi)}(v_{\text{Ego}},\phi) &= p_{V_{\text{Ego}}}(v_{\text{Ego}})p_{\cos(\Phi)}(\phi) \\ &= \frac{1}{\sqrt{4\pi^2\sigma^2_{V_{\text{Ego}}}\sigma^2_{\Phi}(1-\cos^2(\phi))}} \\ &\cdot e^{-\frac{1}{2}\left(\frac{(v_{\text{Ego}}-\mu_{V_{\text{Ego}}})^2}{\sigma^2_{V_{\text{Ego}}}}\left(\frac{(\phi-\mu_\Phi)^2}{\sigma^2_\Phi}+\frac{(-\phi-\mu_\Phi)^2}{\sigma^2_\Phi}\right)\right)}. \end{aligned} \quad (7)$$

The computation of the likelihood $p_{\hat{v}_r}(v)$ that a certain realization v of the velocity for an expected stationary target is being observed for a given parameterization can be obtained by integrating the compound distribution $p_{V_{\text{Ego}}\cos(\Phi)}(v_{\text{Ego}},\phi)$

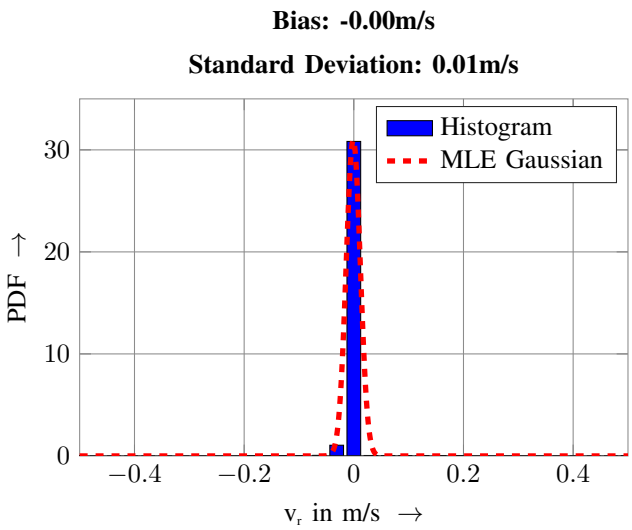

Figure 4: Probability Density Function of observing relative velocity ${}^{R}V_x$ from measurements (histogram) and from Maximum Likelihood Estimation (red)

taking into account the multiplicative influence of the random variables according to eq. 3 (see [12]).

$$p_{\hat{v}_r}(v) = \int_{-\infty}^{\infty} p_{V_{\text{Ego}},\cos(\Phi)}\left(v_{\text{Ego}}, \frac{v}{v_{\text{Ego}}}\right)\left|\frac{1}{v_{\text{Ego}}}\right| \mathrm{d}v_{\text{Ego}} \quad (8)$$

No closed form solution for this integral form is known, so in the following step approximations through numerical integration as well as function approximation are given.

B. Approximate solution of the Marginalization

1) Numerical Approximation: Since realizations of V_{Ego} and Φ can be drawn easily, in this subsection, the results of Monte-Carlo simulations, approximating the probability of drawing v under the condition of a stationary raw target, is given. Here, v_{Ego} and ϕ are drawn according to their distribution densities and associated according to eq. 3 into a single realization of observing the expected radial velocity. After sufficient N draws, here $N = 1000000$, the calculated velocities are represented as normalized histograms (see fig. 5), which gives an approximation of the distribution density $p_{V_{\text{Ego}}\cdot\cos(\Phi)}(v)$.

In this paper the variances are assumed to be invariant from the corresponding mean value, so that the shape of the histogram is modulated exclusively by means of the variable $\mu_{V_{\text{Ego}}}$ and μ_Φ. To illustrate the influence of different parameterizations, all combinations of $\mu_{V_{\text{Ego}}} \in \{0, 20\}\mathrm{ms}^{-1}$ and $\mu_\Phi \in \{0, 90\}^\circ$ are simulated and the resulting marginalizations are shown in fig. 5.

Drawing a representative set from the distribution function $p_{\hat{v}_r}$ and subsequent histogram mapping is not possible on a hardware such as a radar sensor with very limited resources of memory and CPU. Alternatively, an approximation of the distribution density is sought, which represents the true distribution density sufficiently accurately.

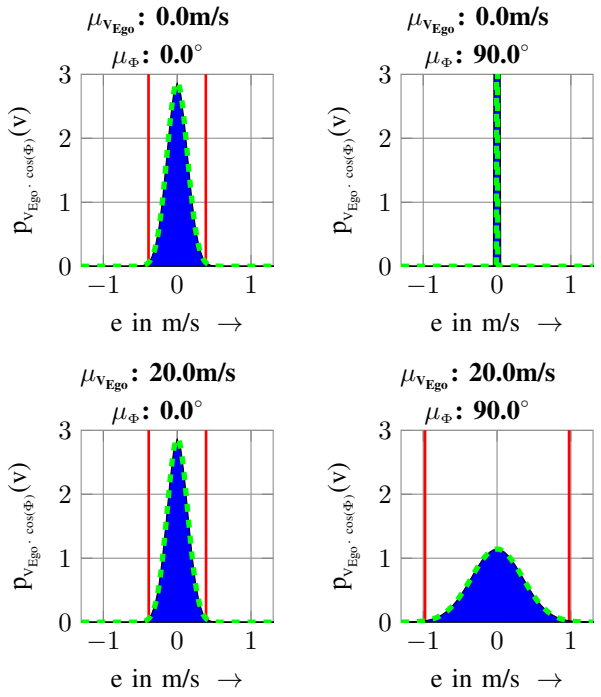

Figure 5: Probability Density Functions through Monte-Carlo simulation (Histogram), the approximated PDF (green) and the confidence intervalls (red) for different parameter values

2) Approximation through Gaussian: Since there is no closed form solution for the marginalization, an approximation is made for given parameter values. As suggested in [13] and [14], the product of two normal-distribution random variables with the mean values μ_x and μ_y and the variances σ_x^2 and σ_y^2 can be approximated by another Gaussian distributions with resulting mean and variance given as

$$E(XY) = \mu_X \mu_Y \tag{9}$$

$$\mathrm{Var}(XY) = \mu_X^2\sigma_Y^2 + \mu_Y^2\sigma_X^2 + \sigma_X^2\sigma_Y^2. \tag{10}$$

To use this knowledge, the distribution density $p_{\cos(\Phi)}(\phi)$ surely must be approximated by a Gaussian distribution beforehand. Therefore, a second order Taylor approximation of cosine at the point μ_Φ is performed and its statistical properties are being computed alternatively. Development beyond the first degree is required, otherwise the variance would disappear at the point $\sin(\mu_\Phi) = 0$.

$$\cos(\Phi) \approx \cos(\mu_\Phi) - \sin(\mu_\Phi)(\phi - \mu_\Phi) - \frac{1}{2}\cos(\mu_\Phi)(\phi - \mu_\Phi)^2 \tag{11}$$

The mean value $\hat{\mu}_\Phi$ of the Taylor approximated distribution $\cos(\Phi)$ can be calculated as

$$\begin{aligned}\hat{\mu}_\Phi &= E[\cos(\mu_\Phi) - \sin(\mu_\Phi)(\phi - \mu_\Phi) - \frac{1}{2}\cos(\mu_\Phi)(\phi - \mu_\Phi)^2] \\ &= \cos(\mu_\Phi) - \frac{1}{2}\cos(\mu_\Phi)\sigma_\Phi^2. \end{aligned}\tag{12}$$

Here we utilize the fact, that the expected value of the sum of two random variables is equal to the sum of the expected value of each individual random variable. Since Φ stems from a Gaussian distribution, its first order central moment disappears and its second order central moments is equal to its variance.

The variance $\hat{\sigma}_\Phi^2$ of the Taylor approximation can be computed as follows

$$\hat{\sigma}_\Phi^2 = \sin^2(\mu_\Phi)\sigma_\Phi^2 + \frac{1}{2}\cos^2(\mu_\Phi)\sigma_\Phi^4. \tag{13}$$

Here it is good to know, that the third order central moment of a Gaussian corresponds to $3\sigma^4$.

The approximated Gaussian distribution of a cosine transformed Gaussian can now be expressed as

$$\hat{p}_{\cos(\phi)}(\cos(\phi)) \sim \mathcal{N}\Bigg(\cos(\phi) \Bigg| \cos(\mu_\Phi) - \frac{1}{2}\cos(\mu_\Phi)\sigma_\Phi^2, \sin^2(\mu_\Phi)\sigma_\Phi^2 + \frac{1}{2}\cos^2(\mu_\Phi)\sigma_\Phi^4 \Bigg). \tag{14}$$

By approximation the distribution $p_{\cos(\Phi)}(\cos(\phi))$ as a Gaussian distributed variable, the parameters of the likelihood $\hat{p}_{\hat{v}_r}(v)$ can now been given according to eq. 9 and 10

$$\begin{aligned}\hat{\mu}_{\hat{V}_r} &= \mu_{V_{\text{Ego}}}\hat{\mu}_\Phi \\ &= \mu_{V_{\text{Ego}}}\left(\cos(\mu_\Phi) - \frac{1}{2}\cos(\mu_\Phi)\sigma_\Phi^2\right)\end{aligned}\tag{15}$$

$$\begin{aligned}\hat{\sigma}_{\hat{V}_r}^2 &= \mu_{V_{\text{Ego}}}^2\hat{\sigma}_\Phi^2 + \hat{\mu}_\Phi^2\sigma_{V_{\text{Ego}}}^2 + \sigma_{V_{\text{Ego}}}^2\hat{\sigma}_\Phi^2 \\ &= \mu_{V_{\text{Ego}}}^2\left(\sin^2(\mu_\Phi)\sigma_\Phi^2 + \frac{1}{2}\cos^2(\mu_\Phi)\sigma_\Phi^4\right) \\ &+ \left(\cos(\mu_\Phi) - \frac{1}{2}\cos(\mu_\Phi)\sigma_\Phi^2\right)^2\sigma_{V_{\text{Ego}}}^2 \\ &+ \left(\sin^2(\mu_\Phi)\sigma_\Phi^2 + \frac{1}{2}\cos^2(\mu_\Phi)\sigma_\Phi^4\right)\sigma_{V_{\text{Ego}}}^2.\end{aligned}\tag{16}$$

To combine the relative velocity of a stationary target given ϕ and v_{Ego} with the radar velocity measurement, we compute the residual e between the measured relative velocity ${}^R v_x$ and the estimated velocity of a stationary target $\hat{v}_r$

$$e = {}^R v_x - \hat{v}_r. \tag{17}$$

The difference of two Gaussians can be given as another Gaussian $p_E(e)$ with mean and variance given in eq. 18 and 19.

$$\mu_E = E({}^R V_x - \hat{V}_r) = \mu_{R_{V_x}} - \hat{\mu}_{\hat{V}_r} \tag{18}$$

$$\sigma_E^2 = \mathrm{Var}({}^R V_x - \hat{V}_r) = \sigma_{R_{V_x}}^2 + \hat{\sigma}_{\hat{V}_r}^2 \tag{19}$$

C. Testing against Hypothesis

The approximated likelihood $p_E(e)$ is now used as a feature for testing the null hypothesis H_0 of stationary radar targets. This hypothesis states that if the radar velocity measurement lies outside the confidence interval associated with the level of significance α, the target is most likely not a stationary target.

This test is described mathematically by the null hypothesis from the following inequalities

$$\text{reject } H_0, \text{ if } e \leq \mu_E - \sigma_E \cdot Q^{-1}(\alpha/2) \quad \text{or } e \geq \mu_E + \sigma_E \cdot Q^{-1}(\alpha/2). \tag{20}$$

The alternative hypothesis H_1 expresses the complementary case, which means that the radar target is a moving object.

III. Results

To generate an statement for the classification accuracy in total $3\,\mathrm{min}$ of real world driving scenarios have been recorded and the raw targets were labeled as stationary or moving. In order to vary the dynamic driving maneuvers, the measurements were varied with different driving velocities and accelerations and a pedestrian walking parallel to the direction of travel as well as stationary objects. Here, a pedestrian was used as a reference for moving objects, since its relative velocity deviates only marginally from stationary objects and thus is particularly challenging. For the labeling task, the ground truth positions of pedestrians thoraxes have been recorded via DGPS-INS and every target within a range of $0.5\,\mathrm{m}$, corresponding to a normal pedestrians step size, around these positions has been labeled as moving, whilst others as stationary.

Since the overall classification accuracy highly depends on the level of significance α, the Receiver Operating Characteristic (ROC) is computed for different parametrizations, see fig. 6.

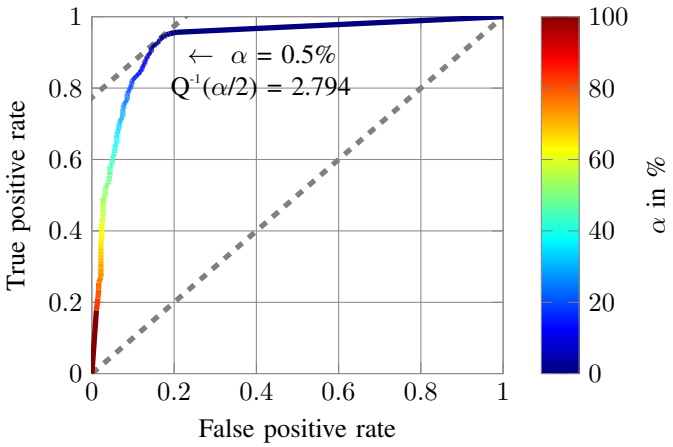

Figure 6: Receiver Operating Characteristic with stationary targets as positives and color coded α

Here, the true positive rate describes the probability of detecting a stationary target, while on the other hand, the false positive rate describes the probability of the misclassification a moving target as a stationary target. The best overall performance, represented by the biggest distance from the ROC curve to the diagonal line, has been recorded at $\alpha = 0.5\%$ corresponding to $Q^{-1}(\alpha/2) = 2.794$, which is used further on.

In fig. 7, a raw target cloud is displayed. Here the raw targets were divided into moving and stationary targets using the hypothesis test. For the scenario, an ego-vehicle equipped with a rear-facing radar sensor passes at a constant speed of about $20\,\mathrm{km\,h^{-1}}$ a parallel walking pedestrian. The targets corresponding to pedestrians are correctly classified as moving targets. Stationary raw targets resulting from ground and curb reflections are mostly identified as static.

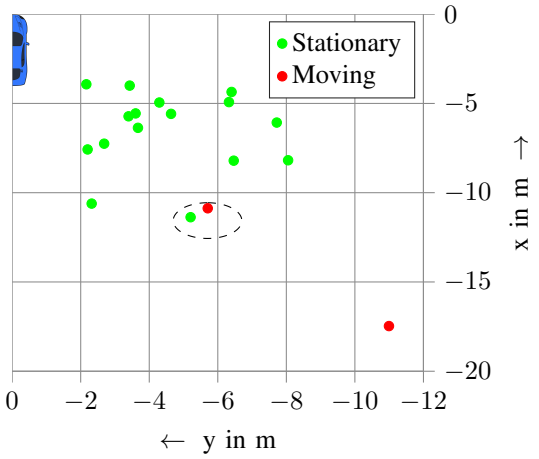

Figure 7: Bird view of radar target point cloud with Ego-Vehicle (car image), walking Pedestrian (black), stationary classified Raw-Targets (green) and dynamic classified Raw-Pargets (red)

To provide an objective statement describing the accuracy of the proposed algorithm, the confusion matrix was computed, see table I.

Table I: Confusion matrix - proposed algorithm, any $|{}^R\phi_S|$

Actual \ Prediction	Moving	Stationary
Moving	88.0%	12.0%
Stationary	6.2%	93.8%

The confusion matrix reflects the subjective perception by which the number of correct classifications clearly dominates. In the confusion matrix it can be observed, that the percentage of misclassified stationary targets is 6.2% which is worse than the expected value of 0.5%, which was parametrized by the level of significance $\alpha = 0.5\%$. After examining the classification of the radar targets in the measuring plane, it was found that the incorrectly classified stationary raw targets mainly result from multipath reflection between the pedestrian holding a highly reflecting corner and the ego-vehicle (see fig. 7 on the right), which have not been hand labeled as moving targets.

We found out, that the main source of misclassification for moving targets is contributed due to the disappearing relative velocity of parallel moving and stationary targets at angle areas of $|\mu_\Phi| \approx 90°$, cf. fig. 1. To quantify this, we computed

the classification accuracy for different observation angles, as can be seen in fig. 8. Also we found, that the degradation

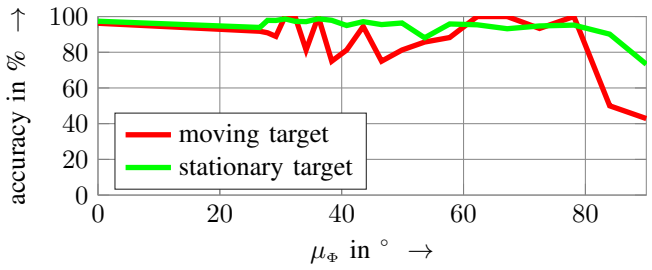

Figure 8: Classification accuracy over observation angles

in classification of moving targets, especially observed at $30° \leq |\mu_\Phi| \leq 50°$, stems from very slow moving or stationary targets within the moving target annotation area which could stem from ground reflections or as very slow moving body parts of the pedestrians like ground touching legs, cf. fig. 7

To compare these results to existing algorithms, the confusion matrix of the RANSAC based classification algorithm from [10] is given, see II.

Table II: Confusion matrix - RANSAC algorithm from [10]

Actual \ Prediction	Moving	Stationary
Moving	87.3%	12.7%
Stationary	6.1%	93.9%

Obvious significant differences in overall accuracy between the algorithms can not be observed, however, we found that the RANSAC algorithm suffers to discriminate moving targets, when the majority of targets stem from moving objects. This is due to the fact, that the algorithm assumes that the majority of targets stem from stationary targets.

Beside the classification accuracy, the computation requirements of both algorithms were tested on our series production radar hardware. It was observed a $> 95\%$ computation time improvement and similar improvements in memory consumption. The cause of this lies in the fact, that the proposed algorithm provides explicit inference, whilst the RANSAC approach needs iterative operation.

For the proposed algorithm, except for the level of significance α which is choosen accordingly to the expected error probability of stationary targets, all required parameters can be measured statistically with respect to the radar and car configuration directly, whereas the RANSAC algorithm requires parametrizing the number of initial target picks, a prescribing targets distance for discriminating moving targets and a maximum number of allowed iterations [10], which need to be chosen heuristically.

IV. Conclusion

In this paper, we have presented a hypothesis test for the identification of moving radar targets in which the statistical properties of radar and ego vehicle speed measurement are taken into account. The aim was to discriminate the raw targets from a single measurement, without having to resort to complex tracking procedures or to utilize demanding RANSAC algorithm. It was shown by means of measurements that the modeling of relevant variables as normal distributed random variables is plausible and the resulting confidence intervals, as discriminating thresholds, for stationary targets are given. On the basis of this, a reliable classification was carried out, even with slow moving objects such as pedestrians. Multipath reflections between moving objects and the ego-vehicle was blamed for occasional misclassifications of stationary raw targets in the vehicle environment. The main accuracy reducing facts for moving targets is the disappearing relative velocity for tangential movement. Also very slow moving targets near pedestrians center have been recorded and annotated as moving, while the classifier marks them as stationary. These slowly moving targets could have stem from ground reflection or as reflections from very slow moving body parts of the pedestrian. However, this misclassification is unintentionally and we see a possible solution in algorithms, which take neighboring targets into account in the classification step and thus be able to give classification to target clusters.

References

[1] R. Farhoud, *Schaetzung des Phasenfehlers von SAR-Rohdaten fuer die Autofokussierung*, Dissertation Univ. Hannover, 2009.

[2] G. Gao and G. Shi and L. Yang and S. Zhou, *Moving Target Detection Based on the Spreading Characteristics of SAR Interferograms in the Magnitude-Phase Plane*, IEEE Transactions on Remote Sensing, 2015.

[3] R. Raney, *Synthetic Aperture Imaging Radar and Moving Targets* , IEEE Transactions on Geoscience and Remote Sensing, 1971.

[4] M. Kirscht, *Detection and imaging of arbitrarily moving targets with single-channel SAR*, in Proceedings of the IEEE Radar, Sonar Navigation, 2003.

[5] The Washington Post, *Google patents a way for self-driving cars to understand a cyclists hand signals*, https://www.washingtonpost.com/news/innovations/wp/2015/05/04/google-patents-a-way-for-self-driving-cars-to-understand-a-\\cyclists-hand-signals/?utm_term=.11181ff9b1bf, "[Visited; 11. April 2017]", 2016.

[6] P. van Dorp and F.C.A. Groen, *Feature-based human motion parameter estimation with radar*, IEEE Transactions on Radar, Sonar & Navigation, 2008.

[7] P. Molchanov, *Radar Target Classification by Micro-Doppler Contributions*, Dissertation Univ. Tampere, 2014.

[8] C. Lundquist and U. Orguner and P. Schoen, *Tracking Stationary Extended Objects for Road Mapping using Radar Measurments*, in Proceedings of the IEEE Intelligent Vehicles Symposium, 2009.

[9] L. Danielsson, *Tracking and radar sensor modelling for automotive safety systems*, University dissertation from Chalmers University of Technology, 2010.

[10] D. Kellner and M. Barjenbruch and K. Dietmayer and J. Klappstein, *Instantanous Lateral Velocity Estimation of a vehicle using doppler radar*, in Proceedings of the 16th International Conference on Information Fusion, 2013.

[11] Y. Sinai, *Central Limit Theorem for Sums of Independent Random Variables*, in Probability Theory: An Introductory Course, 1992.

[12] A. Seijas-Macias and A. Oliverira, *AN APPROACH TO DISTRIBUTION OF THE PRODUCT OF TWO NORMAL VARIABLES*, Report, University of A Corunha, Spain, 2012.

[13] C. Craig, *On the Frequency Function of xy*, Ann. Math. Statist., 1936.

[14] R. Ware and F. Lad, *Approximating the Distribution for Sums of Products of Normal Variables*, Report, Canterbury, England, 2003.